# One and two-phonon Raman scattering from nanostructured silicon

Igor Iatsunskyi [a,b,*], Grzegorz Nowaczyk [b], Stefan Jurga [b], Victoriia Fedorenko [a], Mykola Pavlenko [a], Valentyn Smyntyna [a]

[a] Department of Experimental Physics, Odessa I.I. Mechnikov National University, Str. Pastera 42, 65023 Odessa, Ukraine
[b] NanoBioMedical Center, Adam Mickiewicz University in Poznanul, Umultowska 85, PL 61614 Poznań, Poland

## ARTICLE INFO

## ABSTRACT

Raman scattering from highly/low resistive nanostructured silicon films prepared by metal-assisted chemical etching was investigated. Raman spectrum of obtained silicon nanostructures was measured. Interpretation of observed one and two-phonon Raman peaks are presented. First-order Raman peak has a redshift and broadening. This phenomenon is analyzed in the framework of the phonon confinement model taking into account mechanical stress effects. Second-order Raman peaks were found to be shifted and broadened in comparison to those in the bulk silicon. The peak shift and broadening of two-phonon Raman scattering relates to phonon confinement and disorder. A broad Raman peak between 900 and 1100 $cm^{-1}$ corresponds to superposition of three transverse optical phonons $\sim$2TO ($X$), 2TO ($W$) and 2TO ($L$). Influence of excitation wavelength on intensity redistribution of two-phonon Raman scattering components (2TO) is demonstrated and preliminary theoretical explanation of this observation is presented.

© 2015 Elsevier GmbH. All rights reserved.

## 1. Introduction

Nanostructured silicon is presently of widespread interest because Si is an extremely promising material not only for electronics but optoelectronics, solar cells, sensors etc. Raman scattering has become a standard tool to study the silicon and nanostructured silicon for many years [1–24]. Raman-scattering studies of nanomaterials give us information about energy dispersion, structure, bonding and disorder. The analysis of nanostructures is mainly based on the phonon confinement model in which the finite crystallite size is taken into account by weighting the phonon-scattering efficiency [4–24]. Confinement effects in nanostructures lead to modifications of the electronic, optical and vibrational properties. Unfortunately, if a first-order Raman spectrum of nanocrystalline silicon has been studied extensively, the second-order Raman scattering is investigated marginally [4,9,10].

In the second-order Raman scattering process, two phonons of equal and opposite momentum participate and produce either line or broad continuous spectrum. Zone edge phonons, which appear only in higher-order Raman scattering, correspond to large wave vectors and are sensitive to short-range disorder. The nature of a material, such as crystalline or amorphous, can therefore be ascertained by analyzing the higher-order phonons as well. Study of second-order Raman scattering, in addition to first-order spectra, provides important information on the vibrational modes, energy structure, and morphology of nanostructured materials. Besides, second-order Raman scattering exhibits a higher sensitivity to nanoparticles size than first-order scattering [10].

In this paper we present the one- and two-phonon Raman spectra of nanostructured silicon fabricated by metal-assisted chemical etching. We have measured the Raman frequency shifts and line shapes at room temperature. We focused on the changes in the second-order Raman scattering. New effect dealing with second-order Raman scattering was found.

## 2. Experimental procedure

### 2.1. Nanostructured silicon fabrication

The nanostructured silicon samples were fabricated using a metal-assisted chemical etching process (MACE) [25–27]. The MACE exhibits good process controllability to generate various nanostructured silicon surface morphologies. Similar to electrochemical etching to create porous silicon, MACE acts as a localized electrochemical etching process in which local electrodeless etching occurs at the metal/silicon interface, each nanometer-sized

* Corresponding author at: NanoBioMedical Centre, Adam Mickiewicz University, 85 Umultowska str., 61-614, Poznan, Poland. Tel.: +48 731308173.
E-mail addresses: yatsunskiy@gmail.com (I. Iatsunskyi), cnbmadm@amu.edu.pl (G. Nowaczyk).

metal particle acts as a local cathode and the silicon surface acts as an anode. The metal particles are critical in the process to promote $H_2O_2$ decomposition and cause electron–hole injection into the silicon surface; silicon is dissolved by HF to create pits or other nanostructures on the surface.

Monocrystalline p-type Si samples with resistivity of 0.005 Ohm cm (*sample A*, *B*) and with resistivity of 80 Ohm cm (*sample C*, *D*), after standard RCA cleaning, were cleaned with acetone and deionized water via ultrasonic cleaning. A thin oxide layer was formed, and the surface became hydrophilic. This oxide layer was removed by dipping the samples into a dilute HF solution. The silver particles, which act as catalysts to assist the etching of silicon, were deposited on Si samples by immersion in 0.23 M HF and $10^{-3}$ M $AgNO_3$ metallization aqueous solutions. The time of immersion was varied – 40 s for sample A and sample C; and 200 s for sample B and sample D. After the electroless metallization, the wafers were etched in aqueous solutions containing HF (40%), $H_2O_2$ (30%), and ultrapure $H_2O$ at ratio concentration – $H_2O_2/H_2O/HF = 10/80/40$, for 30 min. After etching, the samples were etched in $HNO_3$ solution to remove silver particles and then were cleaned with deionized water and blown dry with nitrogen. The etching and immersion procedures were performed at room temperature.

### 2.2. Surface morphology characterization

Structural properties of porous silicon prepared by metal-assisted chemical etching have been investigated by Scanning Electron Microscopy (SEM) – Jeol 7001TTLS and Atomic Force Microscope (Bruker company) BioScope Catalyst. AFM measurements were carried out in contact mode. Using AFM and SEM, we could characterize the shape and sizes of nanostructures, their distribution and other parameters of morphology. In order to determine mechanical stresses of obtained structures we used X-ray diffraction analysis. X-ray diffraction studies were performed using Empyrean (PanAnalitical) diffractometer.

### 2.3. Raman measurement

Raman scattering measurements were performed using a Renishaw micro-Raman spectrometer equipped with a confocal microscope (Leica). The samples were measured in backscattering geometry with a spectral resolution better than $1.0 \, cm^{-1}$. The incident light was not polarized; also the detection setup contained no polarization filters. The Raman scattering spectra were excited by 488 nm, 514 nm and 633 nm. The beam was focused on the samples with a 50× microscope objective with a numerical aperture of 0.4. The incident optical power was changed by using neutral density filters in the beam path. The minimum power for which a signal could be measured was limited by the signal to noise resolution of the detector in the spectrometer. All measurements were performed at room temperature in ambient atmosphere.

## 3. Results and discussions

### 3.1. Morphological study of nanostructured silicon

Fig. 1(A)–(D) are the images of scanning electron microscopy, which show the surface morphology of nanostructured silicon samples fabricated by MACE. Samples A and B have mostly the porous structure. This morphology shown in images indicates pores of different sizes depending on the chemical procedures. On the other hand, AFM studies of that samples show the presence of nanometer-sized pyramids (hillocks) between the macropores. These hillocks apparently correspond to Si nanocrystallites, whereas the hollows between them correspond to the narrow (nanometer) pores on the surface. The lateral dimensions of the hillocks, which were determined from AFM images as their largest linear dimensions at a base, are in the range of 15–20 nm. The
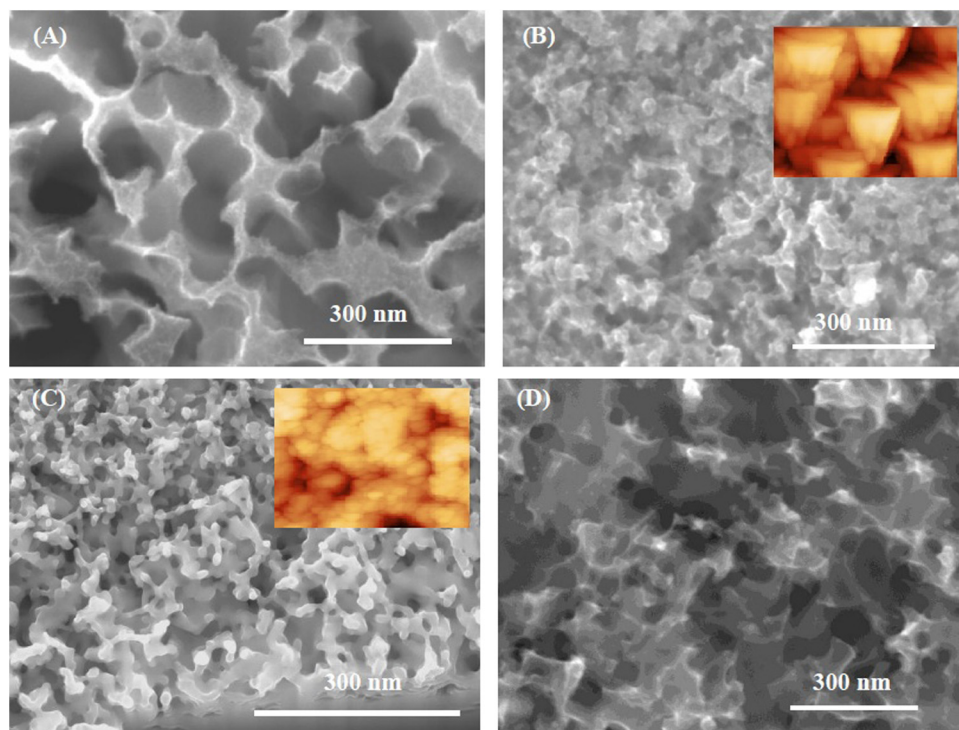


**Fig. 1.** SEM images of nanostructured silicon (insets are AFM images): Ag particles were deposited on Si samples by immersion in 0.23 M HF and $10^{-3}$ M $AgNO_3$ metallization aqueous solutions. The time of immersion was varied – 40 s for sample (A) and sample (C); and 200 s for sample (B) and sample (D). Etching solution contained HF (40%), $H_2O_2$ (30%), and ultrapure $H_2O$ at ratio concentration – $H_2O_2/H_2O/HF = 10/80/40$, for 30 min.

**Table 1**
Silicon phonon frequencies.

| Physical property | Phonon frequencies (in units of cm$^{-1}$) |
| --- | --- |
| LTO ($\Gamma$) | 517–519 |
| TA ($X_3$) | 149–151 |
| LAO ($X_1$) | 410–411 |
| TO ($X_4$) | 460–464 |
| TA ($L_3$) | 113–115 |
| TA ($\Sigma$) | 230 |
| LA ($L_2$) | 377–379 |
| LO ($L_1$) | 420 |
| TO ($L_3$) | 490 |
| TO ($W$) | 470 |

sizes of hillocks increase down to the bottom of pores. It should be noted that the actual lateral dimensions of the elements of the structure are smaller than the dimensions of the AFM images by approximately the doubled radius of the probe tip.

Samples C and D have mostly the "coral-like" structure similar to nanowires with different orientation. Wires have approximate dimensions lying in the range of 10–25 nm. AFM shows mostly the cauliflower-like structure. This morphology shown in 2D images indicates several particles (granules) embedded in each grain (Fig. 1(c) inset). However, the shapes, as well as arrangement of the grains, were found to be different.

All these results confirm that different morphologies can be produced by varying either the dopant level and, of course, the type of etchant and deposition solution.

### 3.2. Raman scattering investigations of nanostructured silicon

Under normal conditions (standard pressure and temperature), silicon crystallizes in a diamond lattice structure, which belongs to the $O_n^7$ space group. The diamond structure of silicon allows only one first-order Raman active phonon of symmetry $\Gamma_{25}$ located at the Brillouin zone (BZ) center corresponding to a phonon wavevector $520.0 \pm 1.0$ cm$^{-1}$ with the full width at half maximum (FWHM) – 3.5 cm$^{-1}$. In order to interpret other Raman peaks, Table 1 shows more important phonon frequencies of silicon [1–5,27].

Raman scattering spectra of samples 1–4 are shown in Fig. 2, for an incident laser power of 10 mW. For all samples one can notice the quite similar Raman spectrum. High peak at 518–519 cm with the FWHM of 8.5–15 cm$^{-1}$ can be seen in the Raman spectrum of nanostructured Si. The intensity of the first-order scattering which is due to the optical phonons (TO, LO) at the center $\Gamma$ point of the BZ, as was mentioned above, is much stronger in comparison with that from the initial Si wafer. In comparison with the first-order optical phonon peak of c-Si, the corresponding Raman peak of nano-Si has very small frequency down-shifted, its linewidth broadened and its line shape becomes asymmetric with a little tail on the low-energy side extending to 470–480 cm$^{-1}$ for all samples what indicate on partial amorphous-like structure. The first-order spectrum from bulk Si single crystal represents scattering by optical phonons with quasimomentum $\mathbf{q} = 0$ because of its conservation in an infinite lattice. Studies of the morphology and structure of nano – Si by SEM/AFM has revealed the presence of nanostructures with dimensions on a nanometer scale (Fig. 1). The limitation of the translation symmetry leads to relaxation of this selection rule, and phonons with quasimomentum out of the region around the $\Gamma$ point determined by the size of the crystallite can contribute to the scattering. Due to the decrease in the frequency of optical phonons with $\mathbf{q}$ in the vicinity of the BZ center, the Raman line of a spectrum from nanocrystalline material is shifted to lower energies and broadened. But comparing our experimental data with references one should conclude that there are additional reasons of the red-shifting and broadening. It is well known that effects of sample
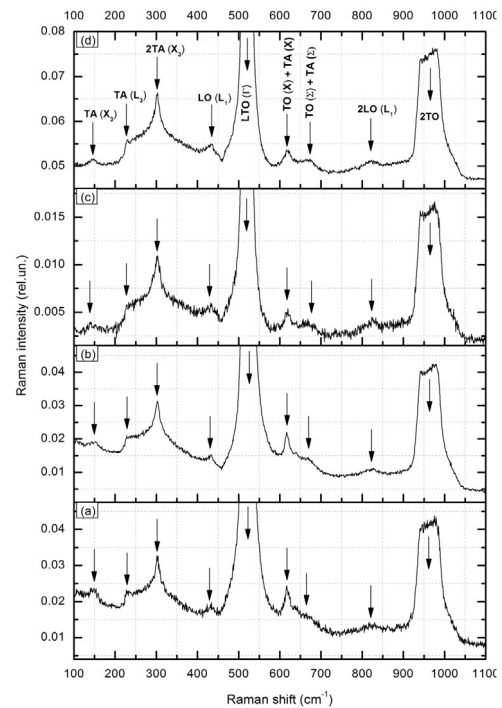


**Fig. 2.** Normalized Raman spectrum of Si nanostructures taken with a 514 nm laser. (A)–(D) – sample, respectively.

heating caused by laser radiation, compressive stress and defects give rise to a frequency shift of the Raman peak [8,11,14,18,21,22]. Therefore, it is necessary to take into account the relative contributions of different mechanisms to the Raman shift and broadening if one need to obtain more precise results for peak line shape.

Khorasaninejad et al. showed that the main reason of red-shifting, but not the peak broadening, is heating effect [22]. They also showed that if confinement effects take place the red-shifting would be approximately 1–2 cm$^{-1}$ which corresponds to our case. Regarding the impact of compressive stress and defects we can estimate it taking into account the following equations [3]

$$\frac{\delta\omega}{\omega} = -3\gamma\frac{a_{PS} - a_0}{a_0},$$ (1)

where $\delta\omega$ is the peak width, $a_{PS}$ is the lattice constant of porous silicon (PS) nanostructures, and $\gamma \approx 1.0$ is the Gruneisen constant. The derived values of strain $a_{PS} - a_0/a_0$ can be estimated from X-ray diffraction analysis. We have obtained this value and it turned out to be an order of $10^{-3}$ for different samples.

Campbell and Fauchet [23] developed a quantitative model that calculates the Raman spectrum of PS as depending on the size $L$ and on the shape of the porous silicon crystallites. If PS is modeled as an assembly of quantum wires, the phonon confinement is assumed to be two dimensional, while if the PS is modeled as an assembly of quantum dots, the confinement is three dimensional. The Raman spectrum is given by:

$$I(\omega) \cong \int_{BZ} \frac{d^3q \left|C(0, q)\right|^2}{(\omega - \omega(q))^2 - (\Gamma_0/2)^2};$$ (2)

where

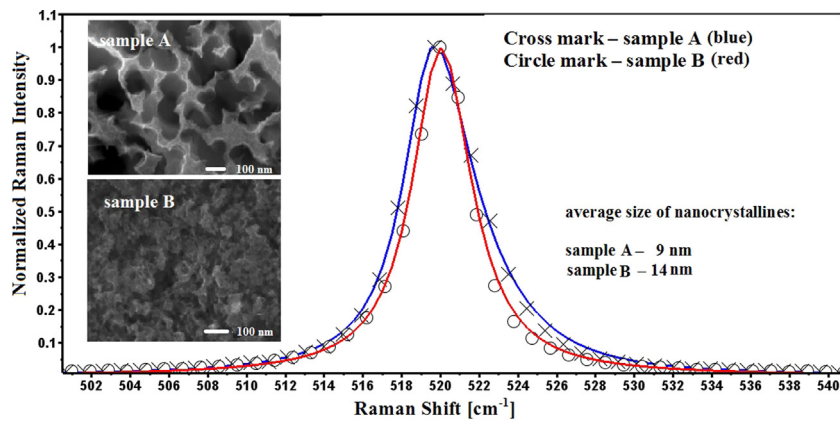$$\left|C(0, q)\right|^2 = \exp\left(-\frac{q^2 L^2}{16\pi^2}\right);$$ (3)

**Fig. 3.** Experimental and calculated curves of nanostructured silicon surface (samples A, B).

The first-order Raman spectrum $I(\omega)$ is thus given by:

$$I(\omega) \cong \int_{BZ} \frac{4\pi q^2 \exp(-(q^2 L^2)/(16\pi^2))d^3 q}{(\omega - \omega(q))^2 - (\Gamma_0/2)^2}; \qquad (4)$$

where $\Gamma_0$ is the natural linewidth for c-Si at room temperature but we should add to this value linewidth corresponding to compressive stress $\delta\omega$ and $\omega(q)$ is the dispersion relation for optical phonons in c-Si. This expression can be taken as [23]:

$$\omega = \omega_0 - 120\left(\frac{q}{q_0}\right)^2; \qquad (5)$$

Here, $\omega_0$ is the position of the c-Si Raman peak. By specifying the size of the silicon nanocrystallites, from Eqs. (4) and (5) the relation between the peak shift and the linewidth in the framework of the phonon confinement model can be determined. Taking into account the impact of compressive stress and confinement effects we reconstructed the Raman spectrum. The results of calculations are presented in Fig. 3. It can be noticed that values of nanocrystallites sizes obtained from calculations are smaller than from SEM. That can be explained by the limited resolution of the electron microscope.

In contrast to c-Si, one can see the first-order scattering from acoustical phonons at $150\,cm^{-1}$ and optical phonon at $430\,cm^{-1}$. These peaks correspond to TA phonon at $X$ critical points – TA $(X)$ and to LO phonon at $L$ critical points – LO $(L)$, respectively (Table 1). The last peak suggests that nanostructured silicon in some extent is in amorphous form [7,15].

A strong enhancement of multiphonon features occurs for nanostructured silicon. The second order spectrum is much weaker than the first-order peak LTO $(\Gamma)$ with features ranging from 100 to $1100\,cm^{-1}$. The second-order spectrum of transverse 2TA acoustical phonons is clearly observed near $300\,cm^{-1}$. Some authors suggest this peak is corresponding to LA modes [19,23] but there is not accurately confirmation of this fact. Probably we observe the superposition of transverse and longitudinal acoustic modes. Comparing the peak position with the values in the Table 1, we can assume that this peak corresponds to TA overtones at $X$ critical points – 2TA $(X)$. We can also observed few little two-phonon peaks – 2TA $(L)$ at $230\,cm^{-1}$ and 2LO $(L)$ at $830\,cm^{-1}$. Some authors explain the 2LO $(L)$ by some kind of disorder but it still is open question [7,15]. In addition, we also found two obvious peaks of Si nanocrystallines at 630 and $670\,cm^{-1}$ which can be ascribed to the quantum confinement effect of Si. These peaks are composed of contributions from combinations and also from overtones of transverse optical and acoustical modes of different critical points. The peak at $630\,cm^{-1}$ probably corresponds to the combination TO $(X)$ + TA

$(X)$ modes and weaker peak corresponds to TO $(\Sigma)$ + TA $(\Sigma)$ [5,9]. Probably, longitudinal modes are also taking part in these combinations as indicated in some publications [10,15,24]. And finally, there is a broad peak between 900 and $1100\,cm^{-1}$ which is from the scattering of few transverse optical phonons $\sim$2TO phonons. A more detailed discussion of this peak will be further.

Since fundamental phonon modes are shifted and broadened, the second-order modes of nanostructured silicon are also shifted and broadened. In addition to the peaks which can be attributed to the scattering from crystalline material, all spectra of our nanostructured silicon samples, although to different extents, exhibit broadbands.

### 3.3. Wavelengths effect of two-phonon Raman scattering

For second-order scattering, the two phonons involved must have equal but opposite wavevector in order to fulfill momentum conservation. Therefore, the strongest scattered signal is due to phonons where the density of states (DOS) is highest [28]. The intensity of the second order Raman signal strongly depends on the scattering geometry due to symmetry reasons. Our results for second-order Raman scattering are shown in Fig. 4. One can see the Raman spectrum of sample A. The laser power for different wavelengths had approximately the same values less then $10\,mW$ to prevent heating effects. We can see a broad peak between 900 and $1100\,cm^{-1}$ which is from the scattering of few transverse optical phonons $\sim$2TO phonons for different wavelength of the excitation light. To date, there is no consensus about the origin of the broad peak. Some authors argue that this peak is formed by the superposition of two or more optical modes [1–5,9,10,13,15,16]. It can be seen that shape line has a kind of complexity. The Raman peak was split onto separate peaks. The peaks, located at 930–940, 950–960 and $980–985\,cm^{-1}$ have been found. As discussed above, the scattering in second-order reflects the phonon DOS. For bulk silicon, the DOS features few strong singularities due to TO phonon at the $X$-point, the $W$-point and the $L$-point. The shoulder at $930–940\,cm^{-1}$, which is identified as two-TO-phonon overtone at zone-edge point $X$, emerges at $930\,cm^{-1}$ – 2TO $(X)$. The peak at $945–955\,cm^{-1}$, which is identified as two-TO-phonon overtone at zone-edge point $W$, emerges at $940\,cm^{-1}$ – 2TO $(W)$. Furthermore, the peak at $980\,cm^{-1}$ corresponding to 2TO-phonon overtone scattering from the critical point $L$, appears at $980\,cm^{-1}$ – 2TO $(L)$. It was noticed that the 2TO peaks narrow as the size of the nanostructures become larger. It is clear from these results that the 2TO band is affected by confinement effects and shifts toward lower frequency and becomes broader as the dimension of the nanocrystals decreases.
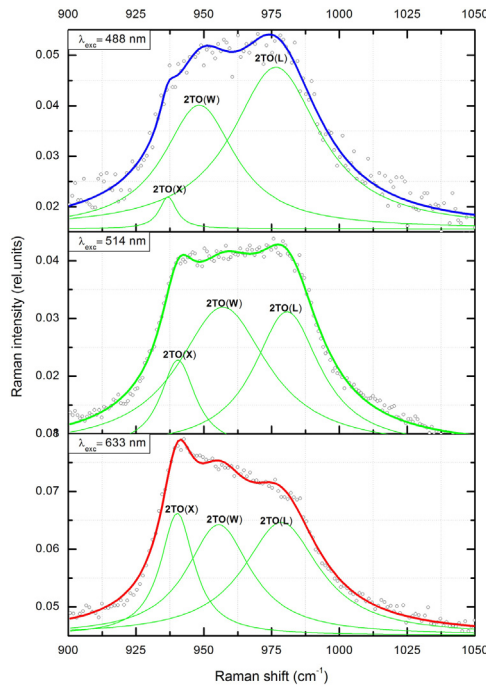
**Fig. 4.** Normalized Raman two-phonon scattering for three different laser wavelengths for sample A. The calculated separate second-order modes are indicated by solid green line curve and the experimental data are plotted as colored bold line. (For interpretation of the references to color in this figure legend, the reader is referred to the web version of this article.)

Exploring the patterns of change in this peak, depending on the wavelength of the excitation light ($\lambda_{exc}$) we found an interesting effect. Changing the $\lambda_{exc}$ leads to an intensity redistribution of Raman scattering components. One can notice that for $\lambda_{exc} = 488$ nm and $\lambda_{exc} = 514$ nm the peaks of 2TO ($L$) and 2TO ($W$) prevail over the 2TO ($X$) mode. For the $\lambda_{exc} = 633$ nm 2TO ($X$) phonon overtone comes maximum and the left shoulder of the broad peak becomes much higher than right shoulder. We compared this result with other publications [1–5,9,10,13,15,16]. Indeed, in other publication one can notice, although to different extents, the same effect. Unfortunately, no one paid attention to this experimental observation.

In order to explain this effect we considered following assumptions: increasing in the intensity of the second-order Raman scattering depends on Raman tensor and effective Raman scattering cross-section. On the other hand, the Raman tensor depends on the probability of interband optical transitions [29,30]. Photons with energies corresponding to the absorption edge for a certain zone-edge point of BZ should have a higher probability of optical transitions and thereby the intensity of Raman peak for certain zone-edge point would increase or decrease its value. The intensity of second-order spectra, $I_2(\omega)$, is related to that of first-order scattering, $I_1(\omega)$, through [30]

$$I_2(\omega) \approx I_1(\omega) f\left(\frac{\hbar\omega_i}{\hbar\omega_g}\right),\tag{6}$$

where $\hbar\omega_i$ – energy of laser photon, $\hbar\omega_g$ – energy equal to band gap width in material. The function $f(\hbar\omega_i/\hbar\omega_g)$ depends in a fairly complex way on the ratio ($\hbar\omega_i/\hbar\omega_g$). If $\hbar\omega_i$ is close to $\hbar\omega_g$, the intensity of second-order Raman scattering becomes resonantly enhanced. The function describing the dependence of the second-order Raman

scattering intensity on the ratio of laser beam energy to band gap width can be written as [30]

$$f\left(\frac{\hbar\omega_i}{\hbar\omega_g}\right) \approx \left[\left(1 - \frac{\hbar\omega_i}{\hbar\omega_g}\right)^{-1.5} + \text{const}\right]^2.\tag{7}$$

It is well known, that the band gap energy increasing with the decreasing of nanostructures size and it results in a growth of $f(\hbar\omega_i/\hbar\omega_g)$ function. Thus, calculation of second-order Raman spectra intensity allows one to estimate the optical energy gap. As far as the intensity of 2TO is concerned, estimated calculations shows that if we use red laser instead of blue one the intensity of 2TO ($X$) peak should increase the intensity approximately in 2.5 times. On the other hand, for peaks (2TO ($L$) and 2TO ($W$)), their intensities should increase approximately in 1.3–1.5 times, that we observed in the experiment. However, the present explanations are tentative, and require further theoretical proof.

## 4. Conclusions

One- and two-phonon Raman scattering characteristics of nanostructured silicon fabricated my metal-assisted chemical etching were investigated and the results are summarized. First-order Raman peak has a small redshift and broadening compared with bulk silicon as predicted by the phenomenological phonon confinement effect for nanostructures. In addition to the fundamental phonon modes, overtone and combinations of modes were also observed and analyzed. Second-order Raman peaks were found to be shifted and broadened in comparison to those in the bulk silicon. A broad peak between 900 and 1100 cm$^{-1}$ corresponds to superposition of three transverse optical phonons $\sim$2TO ($X$), 2TO ($W$) and 2TO ($L$). It was observed the anomalous behavior of the 2TO peaks depending on the wavelength of the excitation light. Our findings are important for characterizing of nanostructures by Raman scattering.

## Acknowledgments

## References

[1] J.H. Parker, D.W. Feldman, M. Ashkin, Phys. Rev. 155 (3) (1967) 712–714.
[2] P.A. Temple, C.A. Hathaway, Phys. Rev. B 7 (8) (1973) 3685–3697.
[3] T. Kamiya, M. Kishi, A. Ushirokawa, T. Katoda, Appl. Phys. Lett. 38 (5) (1981) 377–379.
[4] Min Yang, Darning Huang, Pinghai Hao, Fulong Zhang, Xiaoyuan Hou, Xun Wang, J. Appl. Phys. 75 (1) (1993) 651–653.
[5] H. Tanino, A. Kuprin, H. Deai, Phys. Rev. B 53 (4) (1996) 1937–1947.
[6] C.-H. Cho, Y.-S. Seo, J. Korean Phys. Soc. 33 (3) (1998) 292–296.
[7] M. Ivanda, O. Gamulin, W. Kiefer, J. Mol. Struct. 480/481 (1999) 651–655.
[8] B. Li, D. Yu, S.-L. Zhang, Phys. Rev. B 59 (3) (1999) 1645–1648.
[9] R.-P. Wang, G.-W. Zhou, Y.-L. Liu, S.-H. Pan, H.-Z. Zhang, D.-P. Yu, Z. Zhang, Phys. Rev. B 61 (24) (2000) 16827–16832.
[10] P. Mishra, K.P. Jain, Phys. Rev. B 64 (7) (2001) 073304–073308.
[11] S. Piscanec, M. Cantoro, A.C. Ferrari, J.A. Zapien, Y. Lifshitz, S.T. Lee, S. Hofmann, J. Robertson, Phys. Rev. B 68 (24) (2003) 241312–241316.
[12] N. Korsunska, B. Bulakh, B. Jumayev, L. Khomenkova, V. Yukhymchuk, T. Torchynska, Appl. Surf. Sci. 243 (2005) 30–35.
[13] C. Meiera, S. Lu, V.G. Kravets, H. Nienhaus, A. Lorke, H. Wiggers, Physica E 32 (2006) 155–158.
[14] S.K. Mohanta, R.K. Soni, S. Tripathy, C.B. Soh, S.J. Chua, D. Kanjilal, Physica E 35 (2006) 42–47.
[15] W. Wei, Vacuum 81 (2007) 857–865.
[16] W. Wei, G. Xu, J. Wang, T. Wang, Vacuum 81 (2007) 656–662.
[17] C.-C. Kuo, Opt. Lasers Eng. 47 (2009) 612–616.
[18] D. Abidi, B. Jusserand, J.-L. Fave, Phys. Rev. B 82 (7) (2010) 075210–075221.
[19] Y. Duan, J.F. Kong, W.Z. Shen, J. Raman Spectrosc. 43 (6) (2012) 756–760.
[20] M. Khorasaninejad, J. Walia, S. Saini, Nanotechnology 23 (2012) 275706–275713.

[21] S.-K. Ryu, Q. Zhao, M. Hecker, H.-Y. Son, K.-Y. Byun, J. Appl. Phys 111 (2012) 063513–063521.
[22] M. Khorasaninejad, M.M. Adachi, J. Walia, K.S. Karim, S. Saini, Phys. Status Solidi A 210 (2) (2013) 373–377.
[23] I.H. Campbell, P.M. Fauchet, The effects of microcrystal size and shape on the one phonon Raman spectra of crystalline semiconductors, Solid State Commun. 58 (73) (1986) 9–741;
N.R. Mavilla, C.S. Solanki, J. Vasi, Physica E 52 (2013) 59–64.
[24] Z. Huang, N. Geyer, P. Werner, J. De Boor, U. Gosele, Adv. Mater. 23 (2) (2011) 285–308.
[25] W.K. Kolasinski, Curr. Opin. Solid State Mater. Sci. 9 (2005) 73–83.
[26] C. Chartier, S. Bastide, C. Levy, Electrochim. Acta 53 (17) (2008) 5509–5516.
[27] A. Valentin, J. Sée, S. Galdin-Retailleau, P. Dollfus, J. Phys. Conf. Ser. 92 (2007) 012048–012052.
[28] M. Aouissi, I. Hamdi, N. Meskini, Phys. Rev. B 74 (5) (2006) 054302–054312.
[29] R. Loudon, Adv. Phys. 50 (7) (2001) 813–864.
[30] J.M. Calleja, M. Cardona, Phys. Rev. B 16 (8) (1977) 3753–3761.